

# Digital Pre-Distorted One-Step Phase Retrieval Algorithm for Real-Time Hologram Generation for Holographic Displays

Jinze Sha, Adam Goldney, Andrew Kadis, Jana Skirnewskaja, Timothy D. Wilkinson

## Abstract

In a computer-generated holographic projection system, the image is reconstructed via the diffraction of light from a spatial light modulator. In this process, several factors could contribute to non-linearities between the reconstruction and the target image. This paper evaluates the non-linearity of the overall holographic projection system experimentally, using binary phase holograms computed using the one-step phase retrieval (OSPR) algorithm, and then applies a digital pre-distortion (DPD) method to correct for the non-linearity. Both a notable increase in reconstruction quality and a significant reduction in mean squared error were observed, proving the effectiveness of the proposed DPD-OSPR algorithm.

## Introduction

In a computer-generated holographic projection system, images are generated via the controlled diffraction of coherent light, which is modulated by a spatial light modulator (SLM). Contemporary SLM's can only modulate either phase or amplitude, hence algorithms are needed to compute amplitude-only or phase-only holograms. Among those, phase-only holograms are generally preferred due to inherently higher energy efficiency as there is no intentional blockage of light during modulation. Classic phase retrieval algorithms include direct binary search [1], simulated annealing [2], Gerchberg-Saxton [3], and recent years have also seen numerical optimization methods [4, 5, 6, 7, 8], but these methods are iterative so computation speed is the major challenge. The previous research had demonstrated a real-time computer-generated holography (CGH) method called one-step phase retrieval (OSPR) [9], which was fast enough for real-time holography, but the reconstruction quality still has potential for improvement. Hence, a computationally inexpensive method is needed to improve the reconstruction quality whilst maintaining the real-time property of the OSPR algorithm.

There are several factors contributing to the non-linearities between the reconstruction of hologram and the target image, including the calculation and quantization of the hologram, the modulation of the light and the imperfections in the optical setup. This article proposes the digital pre-distorted one-step phase retrieval (DPD-OSPR) algorithm. The digital pre-distortion (DPD) is carried out on the holographic projection system using holograms computed by the OSPR algorithm by measuring the non-linearity experimentally and applying the according pre-distortion curve on target images. DPD can be done via a one-to-one correction curve or a look-up table (LUT) which allows the relationship between the input and output to be adjusted without any heavy computation.

The intuition of the proposed DPD-OSPR algorithm for CGH comes from the gamma correction method for conventional displays, such as cathode-ray tube (CRT) monitor [10], plasma display panel television (PDP-TV) [11] and thin-film-transistor liquid-crystal display (TFT LCD) [12, 13]. Gamma correction for conventional displays were originally developed to mimic the

perceptual response of human vision [14]. The work presented here is a logical continuation of this approach applied to holographic displays.

## Method

The DPD-OSPR method builds on the OSPR algorithm [9]. The OSPR algorithm relies on the time multiplexing of holograms, exploiting the response time of eyes in order to reduce noise in the replay field, rather than computational optimization of the hologram. As the random noises are averaged by the eye while the target image stays, the perceived noise is lessened by the temporal average detected by the eye [15].

---

### Algorithm 1 One-Step Phase Retrieval (OSPR) algorithm

---

**Input:** Target field  $T$ , Propagation function  $\mathcal{P}$ , Number of sub-frames  $S$

**Output:** List of phase holograms  $H[1 \dots S]$

// Compute a list of hologram sub-frames based on different additive random phase

**for**  $s = 1$  to  $S$  **do**

$E \leftarrow T * \text{RandomPhase}()$

$A \leftarrow \mathcal{P}^{-1}[E]$

$H[s] \leftarrow \mathcal{L}A$

**end for**

// Then display the sub-frames on the SLM sequentially

$s \leftarrow 1$

**while** True **do**

Display( $H[s]$ )

$s \leftarrow s + 1$

**if**  $s > S$  **then**

$s \leftarrow 1$

**end if**

**end while**

---

The OSPR algorithm is described in Algorithm 1, where the propagation function  $\mathcal{P}$  is simply the Discrete Fourier Transform (DFT) for Fraunhofer diffraction [16]. The number of sub-frames  $S$  is set to 24 for this article. The OSPR algorithm generates each hologram sub-frame by taking the inverse Discrete Fourier Transform (iDFT) on the field concatenating the target image with a random phase, and then the phase-only constraint is applied by discarding the amplitude while keeping the phase. After computing the  $S$  subframes, they are then displayed on the SLM sequentially. For real-world SLM with limited bit depth, a further step of quantization on each subframe is needed.

## Experimental setup

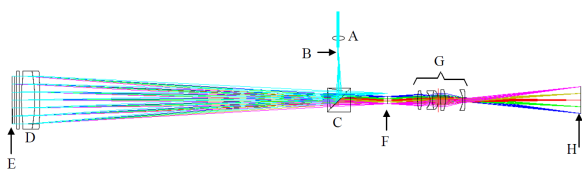


Figure 1. Optical setup [17]

The holographic projector used in this experiment is a Fourier projection system developed by Freeman [17], as shown in Fig. 1. The design is consisted of a diode-pumped solid-state (DPSS) 532 nm 50mW laser source, focussed down by an aspheric singlet (A), the focus of which becomes the diffraction limited point source (B) for the projector. The beam then passes through a polarizing beam splitter cube (C) to a collimating lens (D), which illuminates the SLM (E). The SLM is a binary phase SXGA-R2 ForthDD ferroelectric Liquid crystal on silicon (LCOS) micro-display with a refresh rate of 1440Hz, a pixel pitch of  $13.6\ \mu\text{m}$  and a resolution of  $1280 \times 1024$ . An aperture at point (F) spatially filters out the other orders, leaving only one first order, which is then magnified up by a finite conjugate lens group (G) to produce an image, of the required size, on the screen (H). [17]

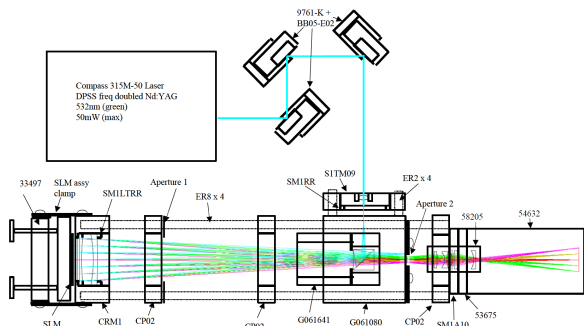


Figure 2. Mechanical components [17]

The mechanical components are listed in Fig. 2 with parts number. The holograms displayed on the SLM are generated using the OSPR algorithm [9], and as the SLM is a binary-phase modulator, each hologram sub-frame needs to be binary quantized. Then each group of the 24 binary-phase hologram sub-frames are encoded as the 8-bit reg, green, blue (RGB) channels of a 24-bit image to interface with the SLM driver electronics. The SLM displays each bit plane sequentially, with ones and zeros mapping to opposing phase modulations at each pixel. The reconstructions were captured using a Canon 550D camera with an EFS 18-55 mm lens. To ensure fair comparison, the camera was set to the same manual setting when comparing each pair of replay fields before and after DPD. It takes  $24/1440 = 1/60$ s to display all 24 sub-frames on a 1440Hz SLM, so the camera shutter speed was set to  $1/30$ s to capture all frames twice. The images captured are in 24-bit RGB colour, which are converted to grey-scale in 8-bit depth when calculating normalized mean squared error (NMSE).

## Determining the DPD curve

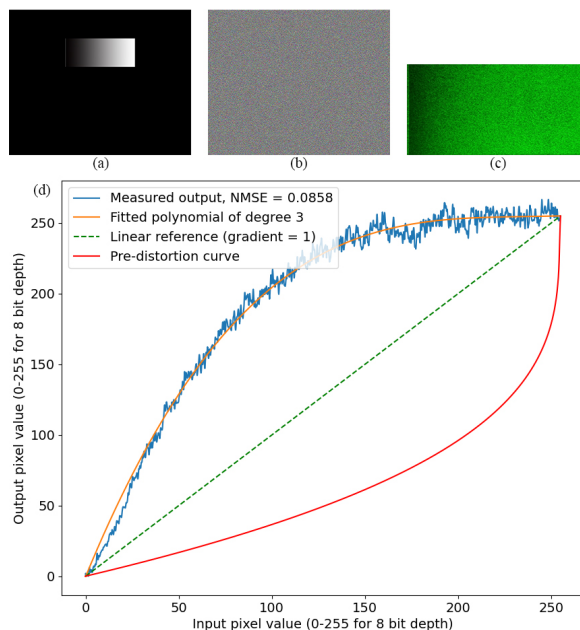
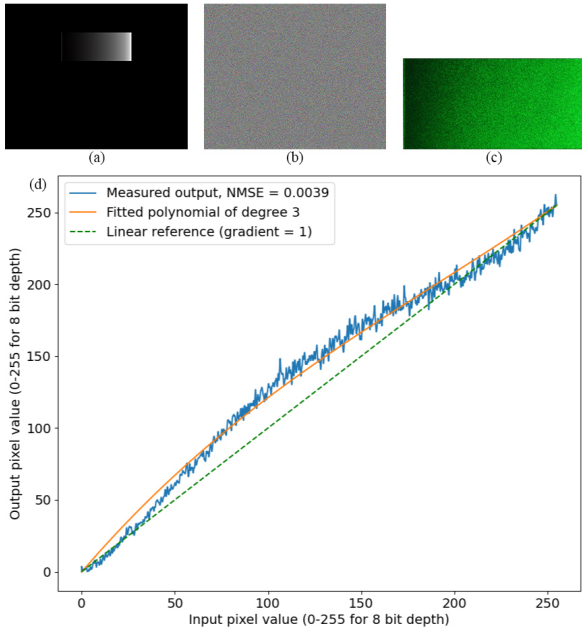


Figure 3. Determining the DPD curve. (a) Input linear grey-scale ramp. (b) Corresponding CGH of (a) with 24-subframe binary phase encoding. (c) Holographic projection replay field of (b). (d) Plot of non-linearity measurement and according pre-distortion curve.

To determine the DPD curve of the holographic projection system, the non-linearity needs to be measured first. The hologram in Fig. 3(b) was first generated using OSPR algorithm for the linear grey-scale ramp of pixel value increasing linearly from 0 to 255, as shown in Fig. 3(a), along with a single pixel white (255) strip at the left end as a fiducial marker to demonstrate the beginning of the grey-scale region [15].

The projection output of the linear grey-scale ramp was then captured and cropped as shown in Fig. 3(c), from which the non-linearity curve was determined, by averaging each column of pixels in the image and discarding the fiducial marker, forming the blue line in Fig. 3(d). A third-order polynomial fit was applied, generating a smoothed non-linearity curve (yellow line in Fig. 3(d)).

There exhibits a high degree of non-linearity. By taking the mean of the square of the error between the measured output (blue line) and the linear reference (green dashed line), the normalized mean squared error (NMSE) of the measured output was calculated to be 0.0858. To correct for the non-linearity, the DPD curve (red line) was formed by inverting the smoothed non-linearity (yellow line) in Fig. 3(d).



**Figure 4.** Validation of DPD curve on the grey-scale ramp. (a) Pre-distorted ramp. (b) Corresponding CGH of (a) with 24-subframe binary phase encoding. (c) Holographic projection replay field of (b). (d) Non-linearity measurement after DPD.

Subsequently, the DPD curve (red line in Fig. 3(d)) was used to adjust the grey-scale ramp, achieving the pre-distorted grey-scale ramp as shown in Fig. 4(a). The according projection output was then captured as shown in Fig. 4(c). By using the same method of averaging columns of pixels, the measured output was plotted in Fig. 4(d). It can be seen that the corrected non-linearity was much closer to linear comparing to the original non-linearity, and the NMSE was calculated to be 0.0039.

	NMSE	Percentage
Before DPD	0.0858	100%
After DPD	0.0039	4.55%

#### Non-linearity results before and after DPD

Hence, as demonstrated in Table 1, DPD achieved a 95.45% reduction in MSE, which was a significant improvement in non-linearity, therefore the DPD curve measured is validated.

#### Applying the DPD Curve

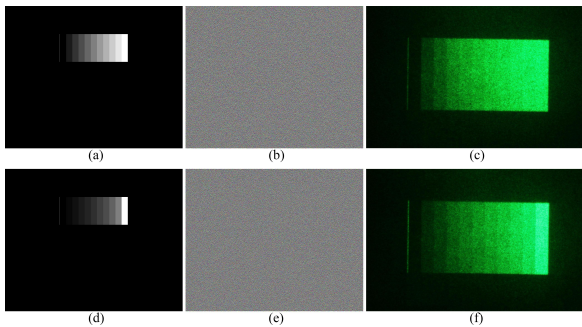


**Figure 5.** Application of DPD on the 10-step strips. (a) 10 strips with equal step of pixel value. (b) CGH of (a). (c) Holographic projection replay field of (b). (d) After DPD of (a). (e) CGH of (d). (f) Holographic projection replay field of (e).

To qualitatively demonstrate the effectiveness of our approach, we project a simple test pattern of a graduated ramp test pattern consisted of 10-step strips in Fig. 5(a), which is commonly employed in gamma-correction calibration of many display systems. As shown in the projection replay field captured in Fig. 5(c), before DPD, the right few strips are barely distinguishable. In comparison, after carrying out DPD, it can be seen that each pair of adjacent strips in Fig. 5(f) are much more distinguishable, qualitatively showing the effectiveness of the DPD method.

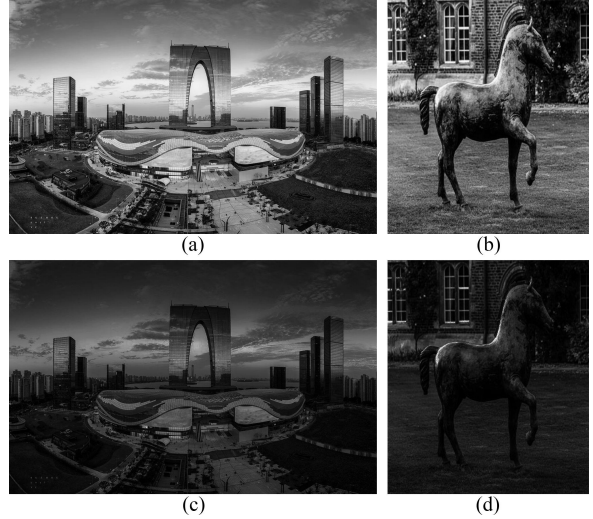


**Figure 6.** Application of DPD on two sample real-word image. (a) Sample image 1: City Scene [18]. (b) Sample image 2: Horse. (c) Sample image 1 after DPD. (d) Sample image 2 after DPD.

Then the DPD curve was applied to the two sample images as shown in Fig. 6 (a) and (b), producing pre-distorted images in Fig. 6 (c) and (d). Holograms were generated for each image using the OSP algorithm and loaded onto the SLM respectively. The according replay fields were captured as shown in Fig. 7.

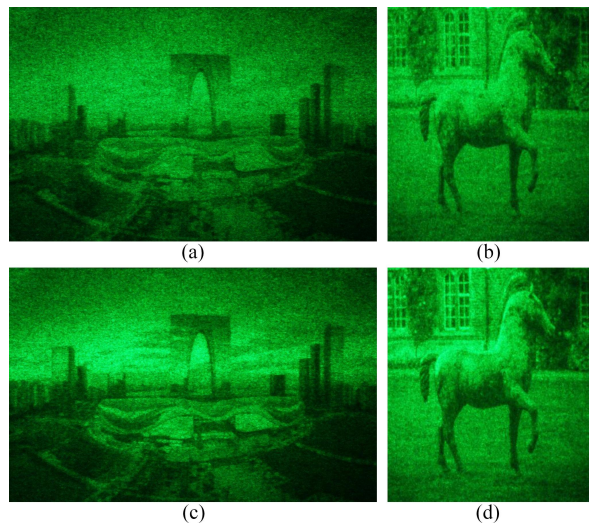


**Figure 7.** Projection output of the two sample images before and after DPD. (a) Replay field of Sample image 1 before DPD (NMSE=0.06139). (b) Replay field of Sample image 2 before DPD (NMSE=0.04309). (c) Replay field of Sample image 1 after DPD (NMSE=0.04920). (d) Replay field of Sample image 2 after DPD (NMSE=0.03635).

The replay fields of the holographic projection of original images are shown in Fig. 7 (a) and (b), and the replay fields of the holographic projection of images after DPD are shown in Fig. 7 (c) and (d).

As shown in Fig. 7(a), it can be seen that, before DPD, the edges between the buildings and the sky were quite ambiguous, with most detail of the sky being lost. In comparison, after DPD, the replay field in Fig. 7(c) provided not only sharper edges between buildings and the sky, but also more detail of clouds in the sky. The NMSE of the replay field for sample image 1 decreased from 0.06139 to 0.04920, which was a 19.86% reduction.

In Fig. 7(b), before DPD, the horse was difficult to distinguish from the background, especially around the horse's back area. But after DPD, as shown in Fig. 7(d), contrast has been significantly boosted and the fine detail around this part of the horse is more evident. The NMSE of the replay field for sample image 2 decreased from 0.04309 to 0.03635, which was a 15.64% reduction.

Sample image 1	NMSE	Percentage
Before DPD	0.06139	100%
After DPD	0.04920	80.15%
Sample image 2	MSE	Percentage
Before DPD	0.04309	100%
After DPD	0.03635	84.36%

#### DPD results for sample images

Hence, as summarised in Table 2, DPD achieved a 19.86% reduction in NMSE for sample image 1 and a 15.64% reduction in NMSE for sample image 2, quantitatively proving the effectiveness of DPD method for CGH of real-world test images using OSPR algorithm.

Lastly, as the DPD is a one-to-one mapping, the computation time is negligible. In practice, the computational overhead is too small to be measured against randomness between subsequent runs. DPD can also be further accelerated in hardware using a hardware LUT, so that the DPD can be carried out instantly. This approach is widely adopted in gamma correction for displays.

## Conclusion

The non-linearity between target image and reconstructed image was measured for the overall holographic projection system by projecting a linear grey-scale ramp. Then DPD was applied to the grey-scale ramp and successfully reduced the MSE by 95.45%. To examine its effectiveness on real world images, the DPD method was applied on two sample images, it was observed that more details were shown in the replay field after DPD, and the MSE's of the two example images were reduced by 19.86% and 15.64%. As the DPD is a one-to-one mapping, the extra computation required is negligible. Hence, we have demonstrated the effectiveness of the proposed DPD-OSPR method to improve reconstruction quality on the existing OSPR algorithm while still keeping its ability for real-time holography.

## Acknowledgments

This work was supported by the Engineering and Physical Sciences Research Council (EPSRC) [EP/S022139/1].

## References

[1] M. A. Seldowitz, J. P. Allebach, and D. W. Sweeney, "Synthesis of digital holograms by direct binary search," *Applied Optics*, vol. 26, 1987.

[2] S. Kirkpatrick, C. D. Gelatt, and M. P. Vecchi, "Optimization by simulated annealing," *Science*, vol. 220, 1983.

[3] R. W. Gerchberg, "A practical algorithm for the determination of phase from image and diffraction plane pictures," *Optik*, vol. 35, pp. 237–246, 1972.

[4] J. Zhang, N. Pégard, J. Zhong, H. Adesnik, and L. Waller, "3d computer-generated holography by non-convex optimization," *Optica*, vol. 4, p. 1306, 10 2017.

[5] S. Liu and Y. Takaki, "Optimization of phase-only computer-generated holograms based on the gradient descent method," *Applied Sciences (Switzerland)*, vol. 10, 2020.

[6] S. Choi, J. Kim, Y. Peng, and G. Wetzstein, "Optimizing image quality for holographic near-eye displays with michelson holography," *Optica*, vol. 8, p. 143, 2 2021.

[7] C. Chen, B. Lee, N.-N. Li, M. Chae, D. Wang, Q.-H. Wang, and B. Lee, "Multi-depth hologram generation using stochastic gradient descent algorithm with complex loss function," *Optics Express*, vol. 29, p. 15089, 5 2021.

[8] A. Kadis, B. Wetherfield, J. Sha, F. Yang, Y. Wang, and T. D. Wilkinson, "Effect of bit-depth in stochastic gradient descent performance for phase-only computer-generated holography displays," pp. 36–40, Society for Imaging Science and Technology, 7 2022.

[9] A. J. Cable, E. Buckley, P. Mash, N. A. Lawrence, T. D. Wilkinson, and W. A. Crossland, "53.1: Real-time binary hologram generation for high-quality video projection applications," *SID Symposium Digest of Technical Papers*, vol. 35, p. 1431, 2004.

[10] X. Guan, S. Jian, P. Hongda, Z. Zhiguo, and G. Haibin, "An image enhancement method based on gamma correction," in *2009 Second International Symposium on Computational Intelligence and Design*, vol. 1, pp. 60–63, 2009.

[11] S. J. Kang and S. I. Chien, "Apl-adaptive inverse gamma correction for improving gray-level linearity of pdp-tv," *Molecular Crystals and Liquid Crystals*, vol. 499, no. 1, pp. 185/[507]–192/[514], 2009.

[12] P.-M. Lee and H.-Y. Chen, "Adjustable gamma correction circuit for tft lcd," in *2005 IEEE International Symposium on Circuits and Systems (ISCAS)*, pp. 780–783 Vol. 1, 2005.

[13] C. A. Párraga, J. Roca-Vila, D. Karatzas, and S. M. Wuerger, "Limitations of visual gamma corrections in lcd displays," *Displays*, vol. 35, pp. 227–239, 2014.

[14] C. Poynton, *Digital Video and HD: Algorithms and Interfaces*. Morgan Kaufmann, 2 ed., 2012.

[15] A. J. Cable, *Real-time high-quality two and three dimensional holographic video projection using the one-step phase retrieval (OSPR) approach*. PhD thesis, Dept. Eng., Cambridge Univ., Cambridge, United Kingdom, 2006.

[16] J. Daintith, *A Dictionary of Physics*. Oxford University Press, 2009.

[17] J. Freeman, *Visor Projected Helmet Mounted Display for Fast Jet Aviators using a Fourier Video Projector*. PhD thesis, Dept. Eng., Cambridge Univ., Cambridge, United Kingdom, 2009.

[18] X. Zhao, "Suzhou center mall," 2017. Suzhou, Jiangsu, China.

## Author Biography

Jinze Sha received his BA and MEng from the University of Cambridge (June 2020). After graduation, he worked for Advanced Micro Devices (AMD) for a year (Aug 2020- Aug 2021). Then he returned to the University of Cambridge to pursue a PhD degree (from Oct 2021). His research has focused on algorithms for computer generated holography (CGH).